Supplement of Atmos. Chem. Phys., 17, 11991–12010, 2017
https://doi.org/10.5194/acp-17-11991-2017-supplement

Atmospheric Chemistry and Physics
Open Access

Supplement of

Modeling of the chemistry in oxidation flow reactors with high initial NO

Zhe Peng and Jose L. Jimenez

Correspondence to: Zhe Peng (zhe.peng@colorado.edu) and Jose L. Jimenez (jose.jimenez@colorado.edu)

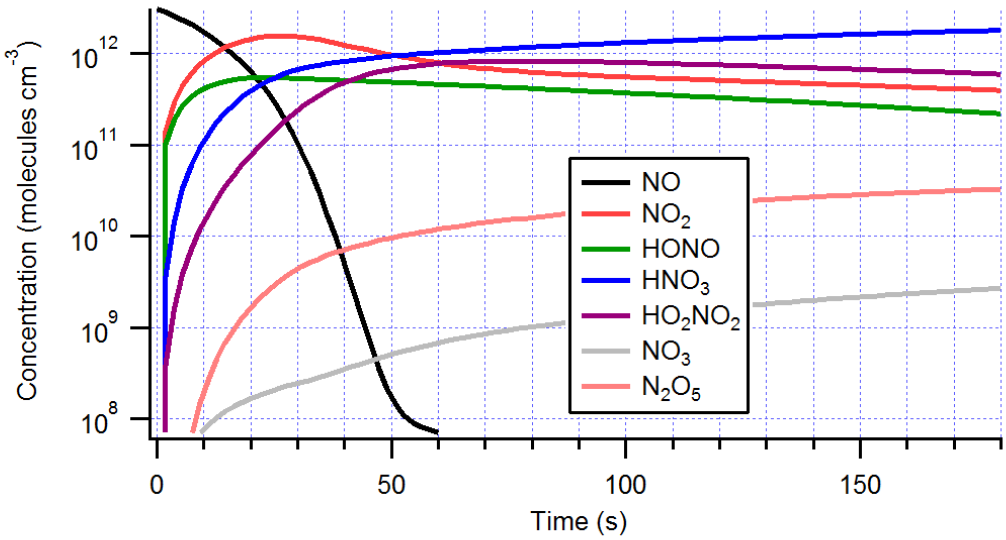

(a) OFR185-iNO (150 ppb NO)

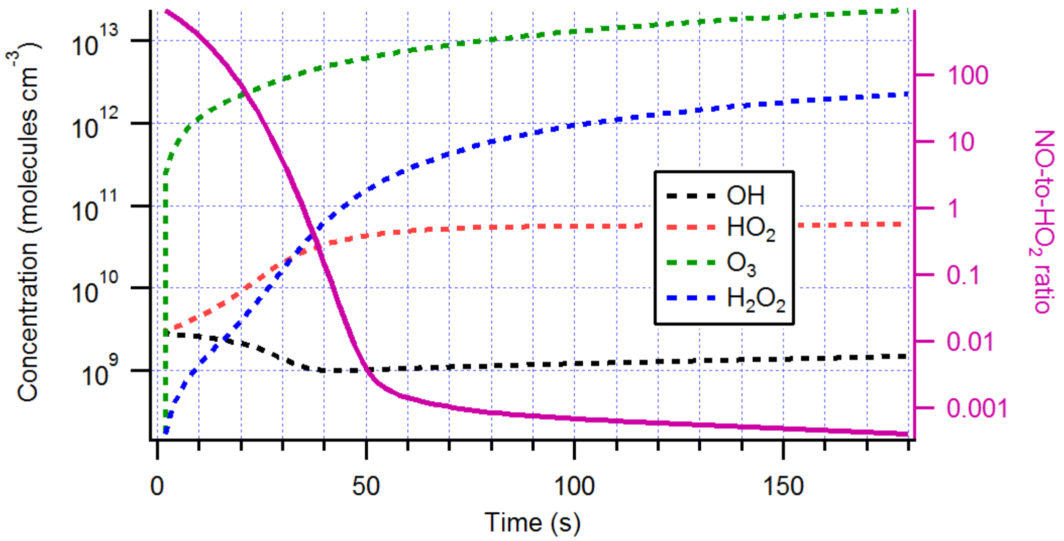

(b) OFR185-iNO (150 ppb NO)

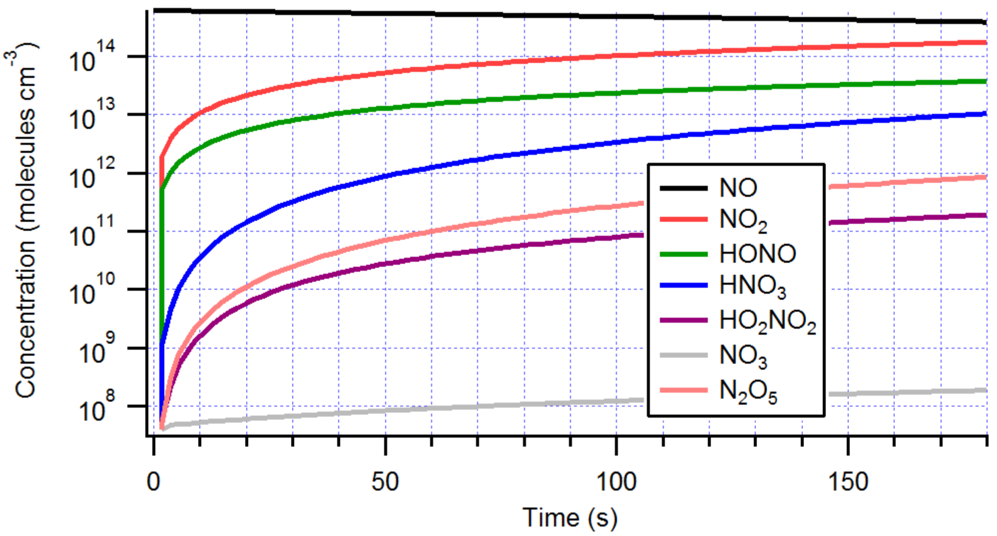

(c) OFR185-iNO (30 ppm NO)

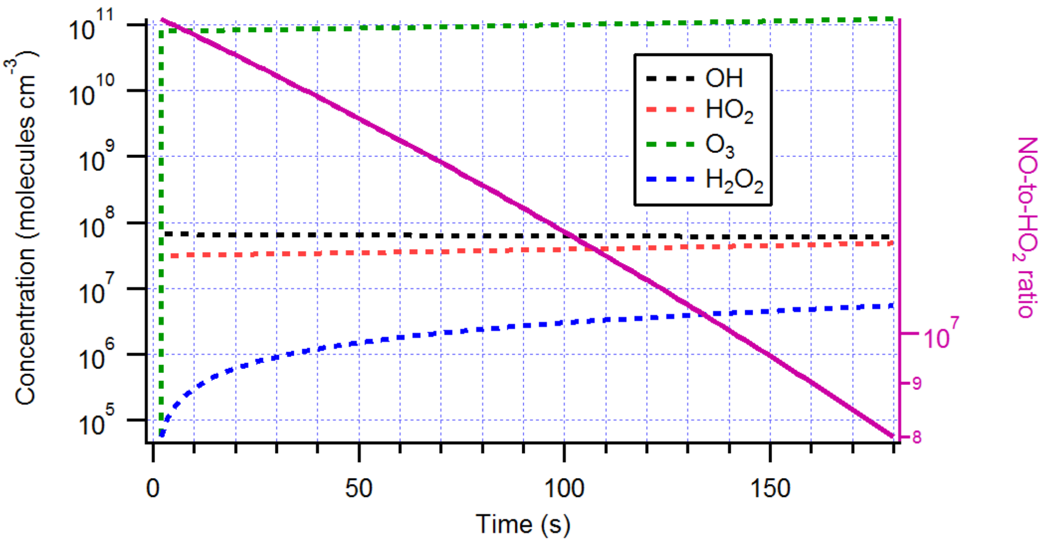

(d) OFR185-iNO (30 ppm NO)

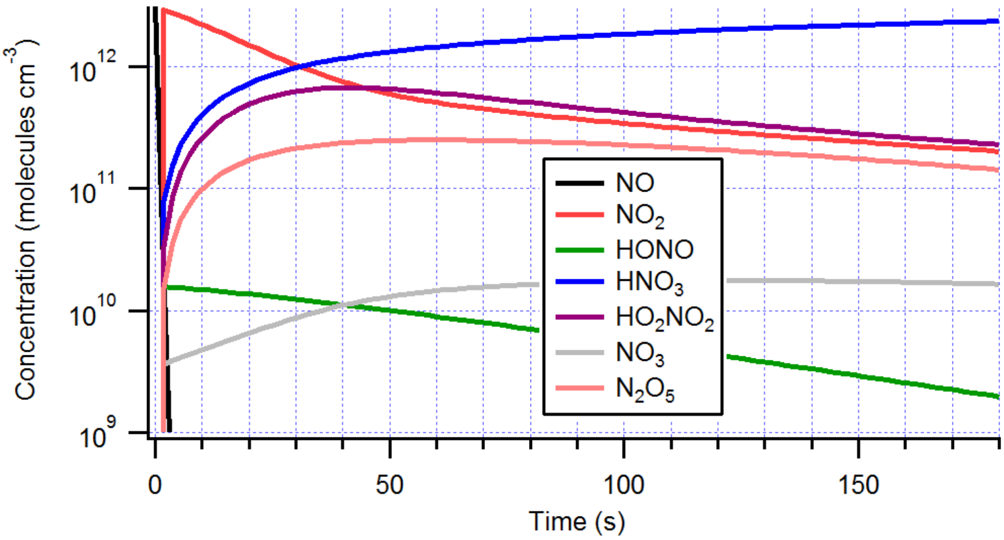

(e) OFR254-iNO (150 ppb NO)

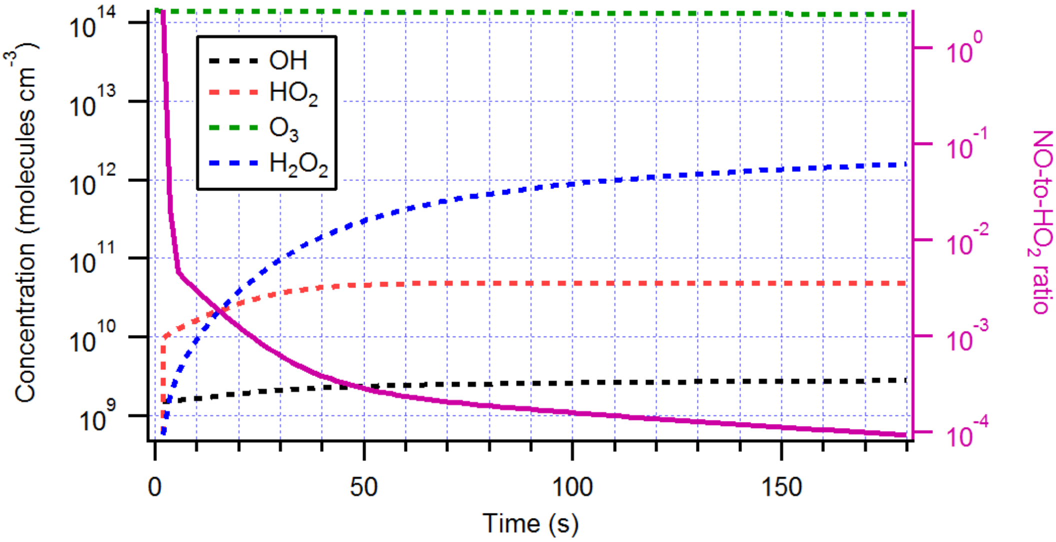

(f) OFR254-iNO (150 ppb NO)

Figure S1. Concentrations of (a, c, e) several NO_y species and (b, d, f) OH, HO_2, O_3, and H_2O_2 and ratio of

NO concentration to that of HO_2 as a function of reaction time in the cases shown in Fig. 1 (OFR185-iNO with 150 ppb initial NO, OFR185-iNO with 30 ppm initial NO, and OFR254-iNO with 150 ppb initial NO).

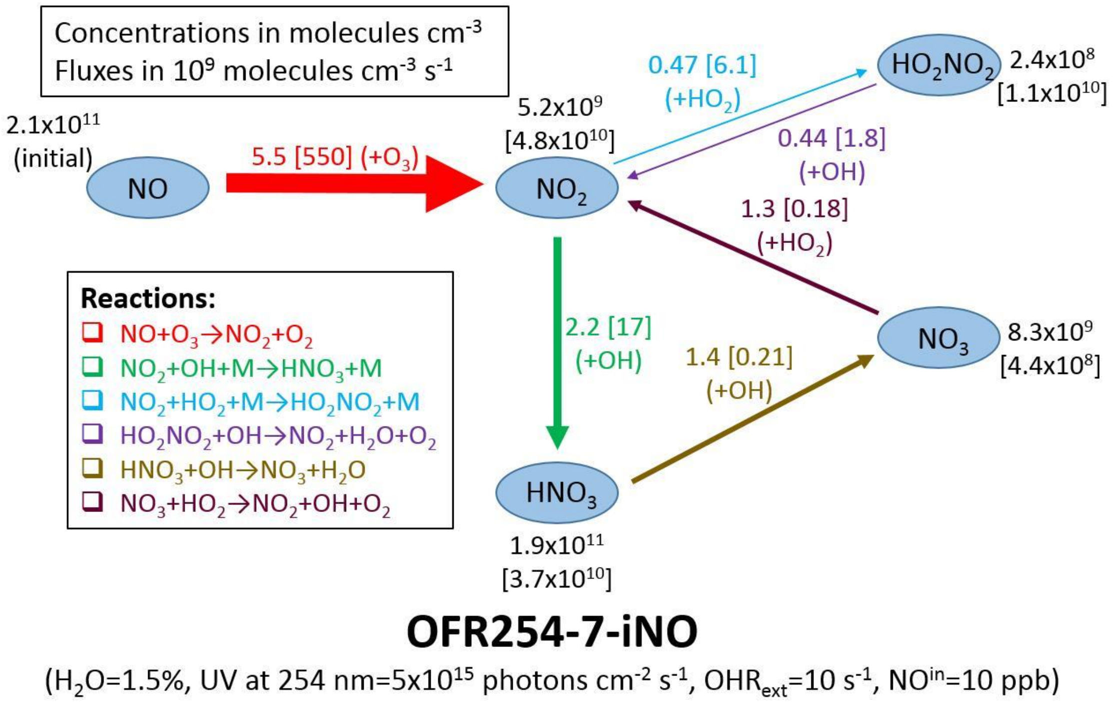

Figure S2. Same format as Fig. 1b, but at a lower initial NO level.

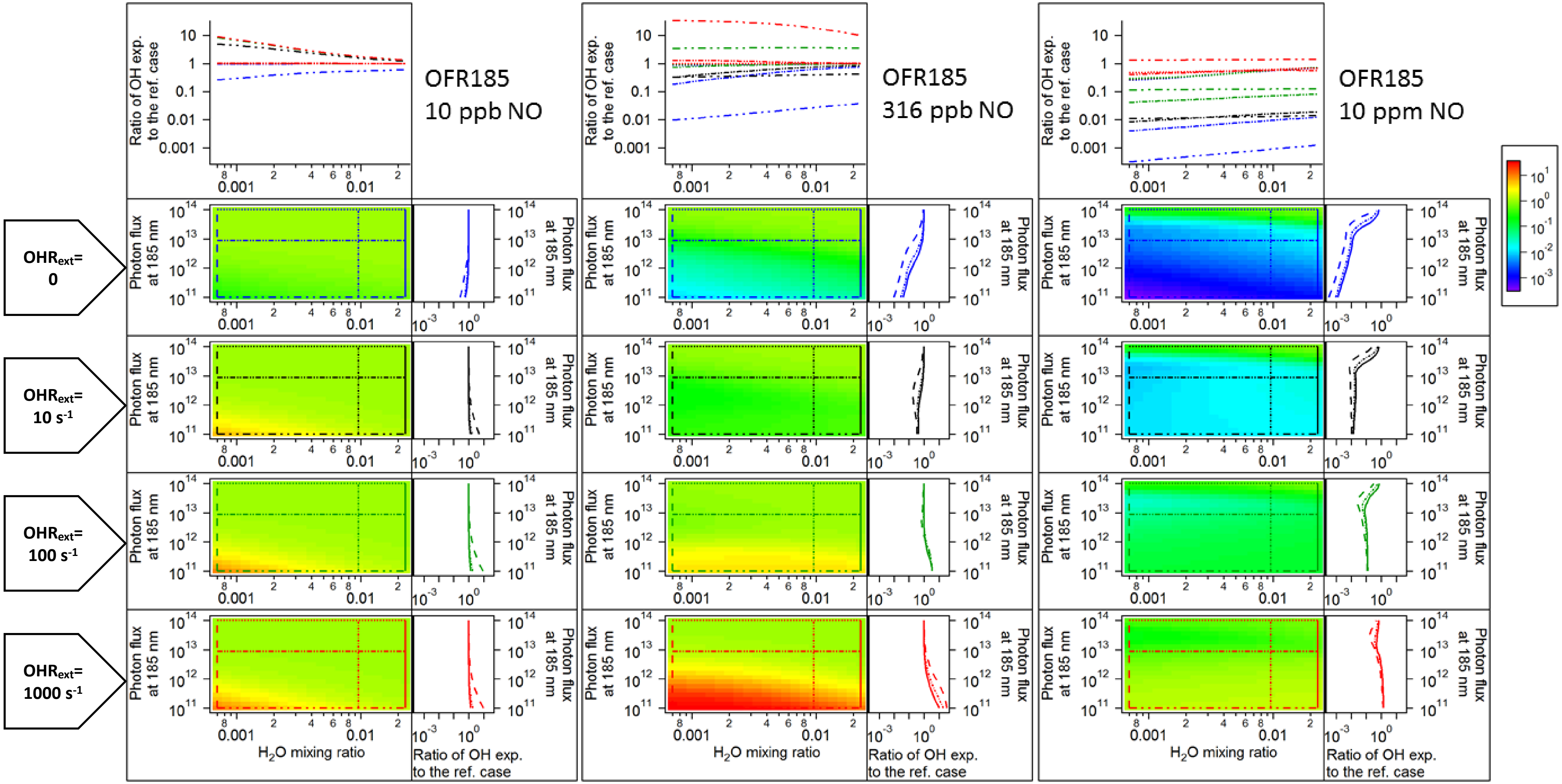

(a) Ratio of OH exposure in the case with input NO to that in the corresponding case (same H_2O, UV, and OHR_{ext}) without input NO for OFR185-iNO

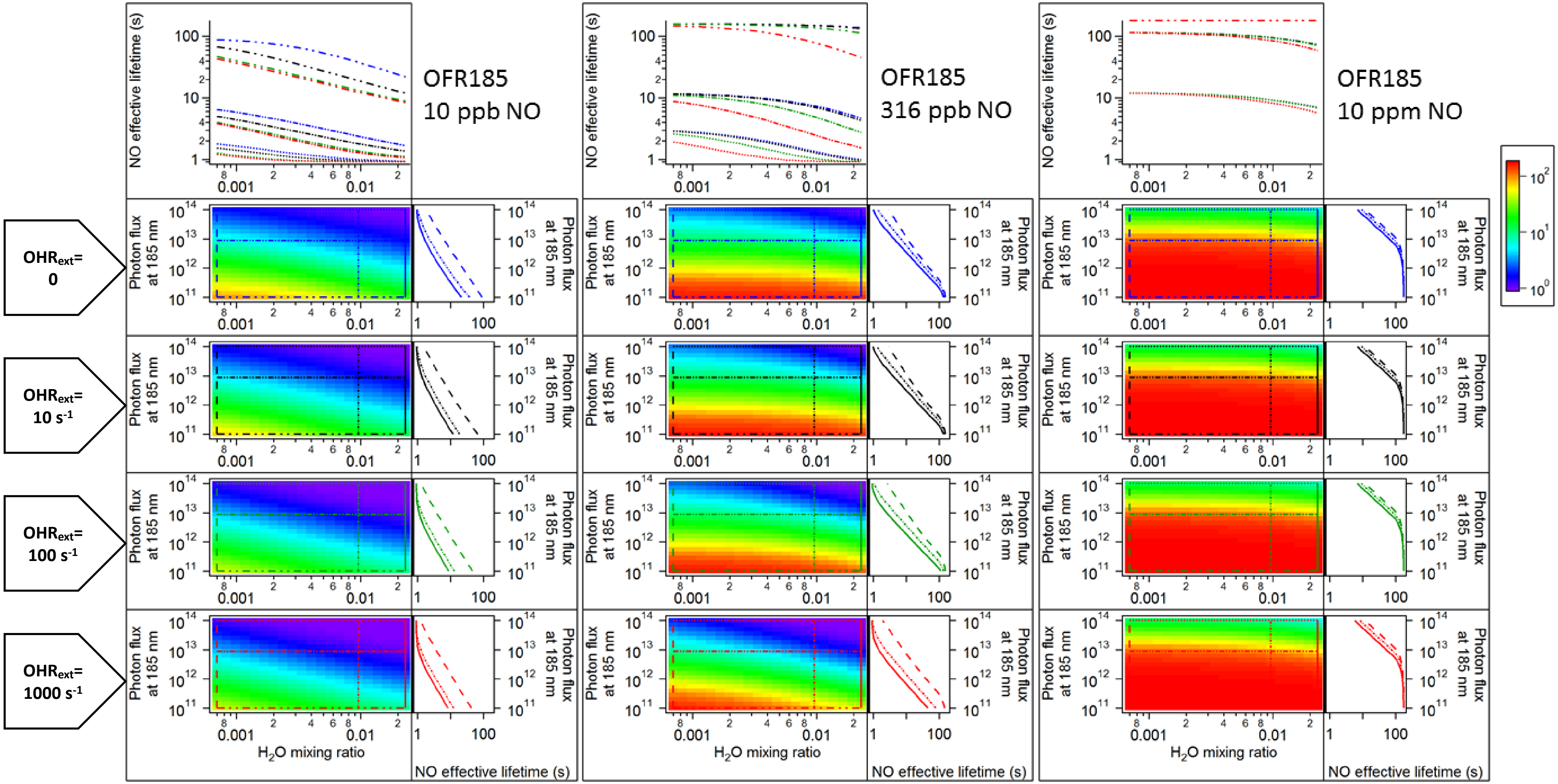

(b) NO effective lifetime for OFR185-iNO

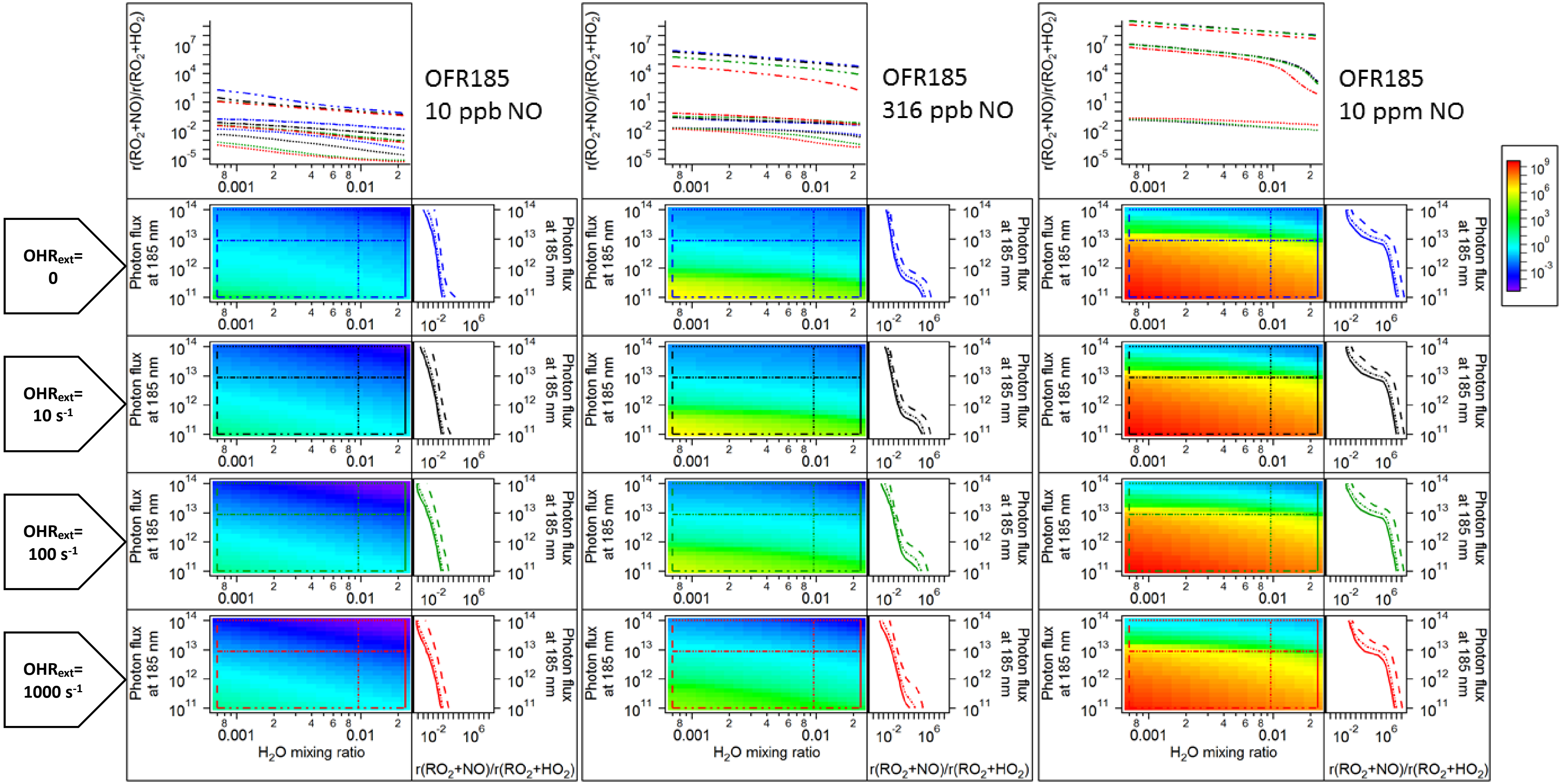

(c) r(RO$_2$+NO)/r(RO$_2$+HO$_2$) for OFR185-iNO

32

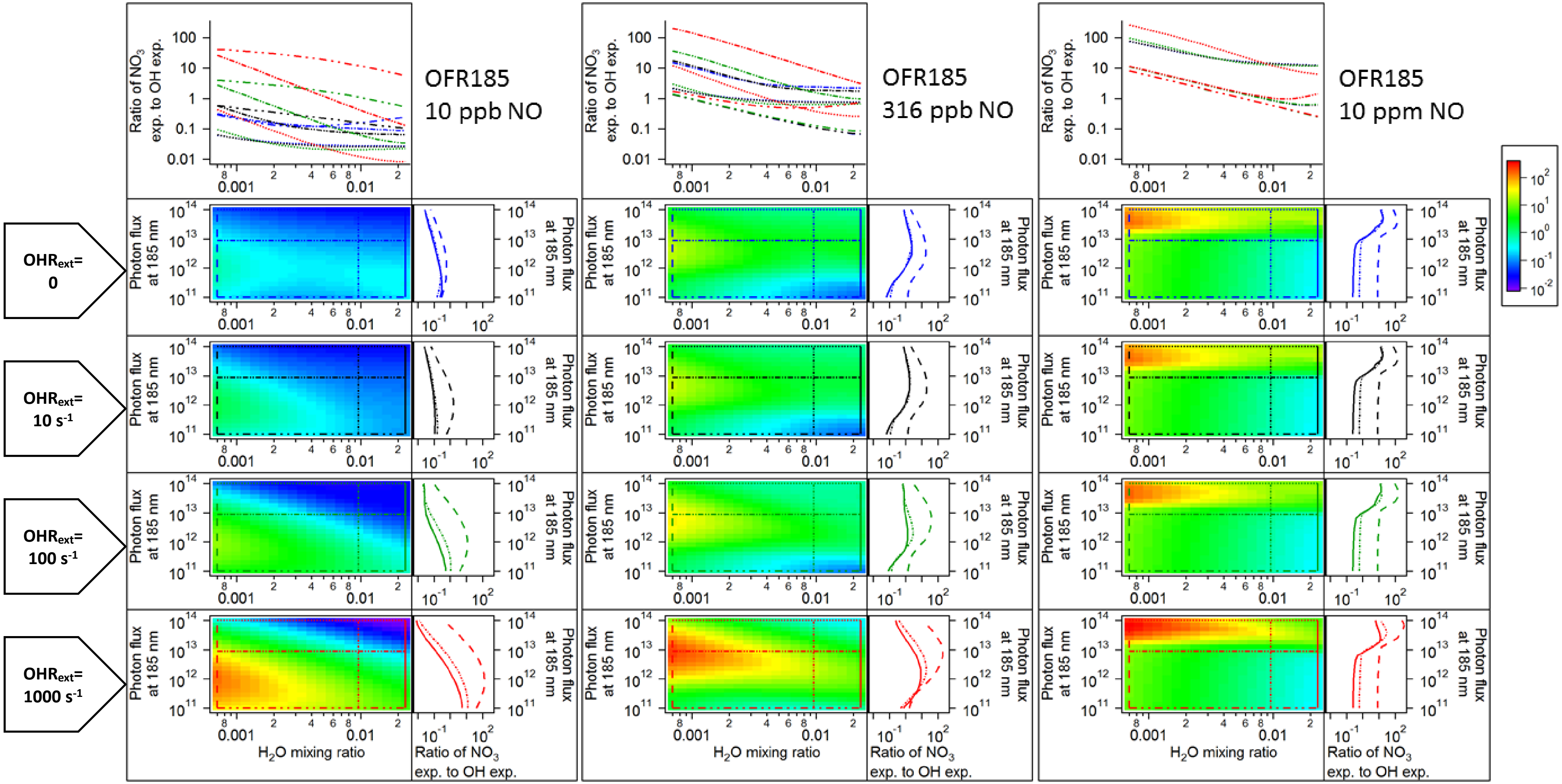

33 **(d) NO₃ exposure/OH exposure for OFR185-iNO**

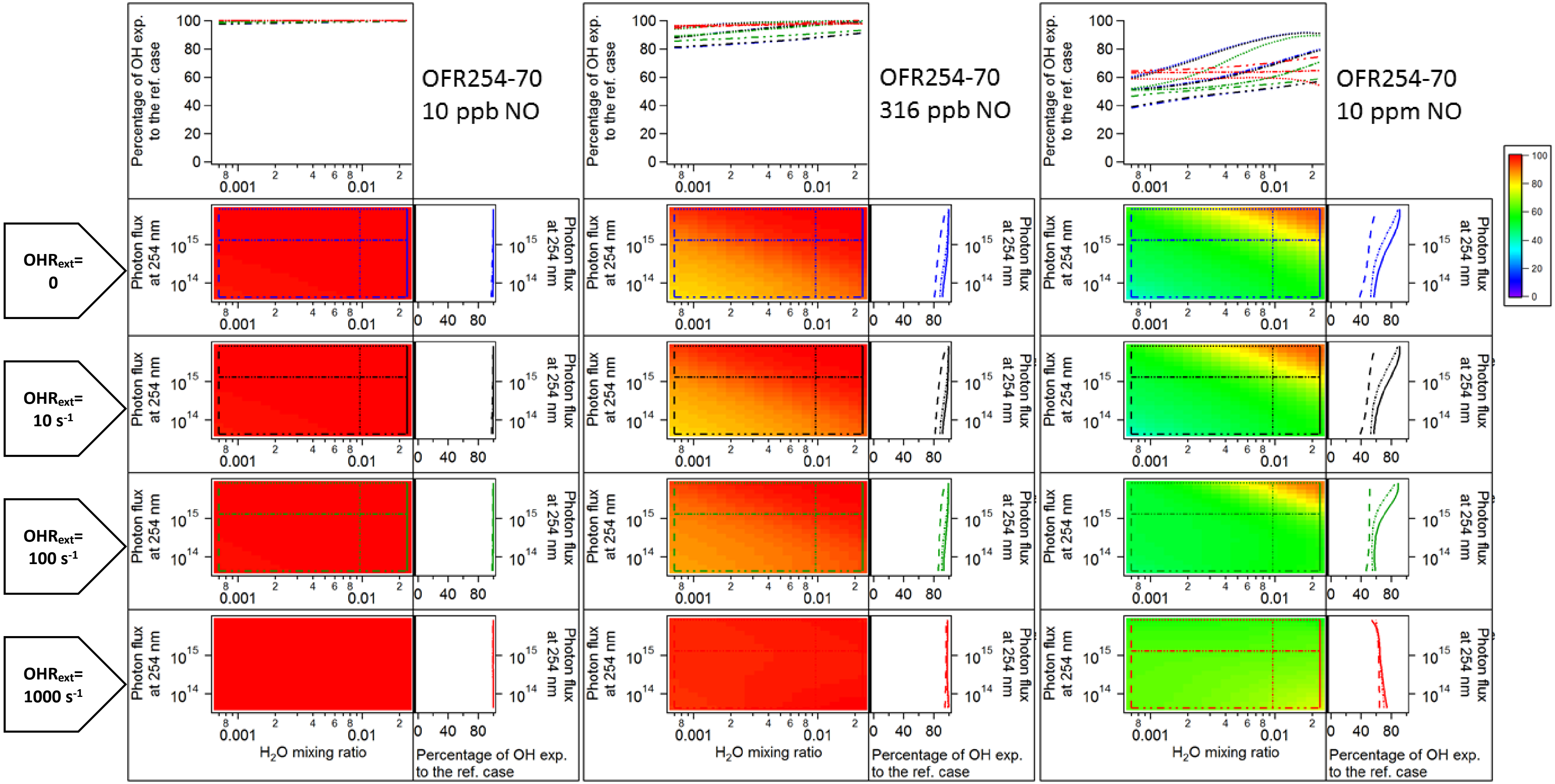

34
35 (e) Ratio of OH exposure in the case with input NO to that in the corresponding case (same H_2O, UV, and OHR_{ext}) without input NO for OFR254-70-iNO

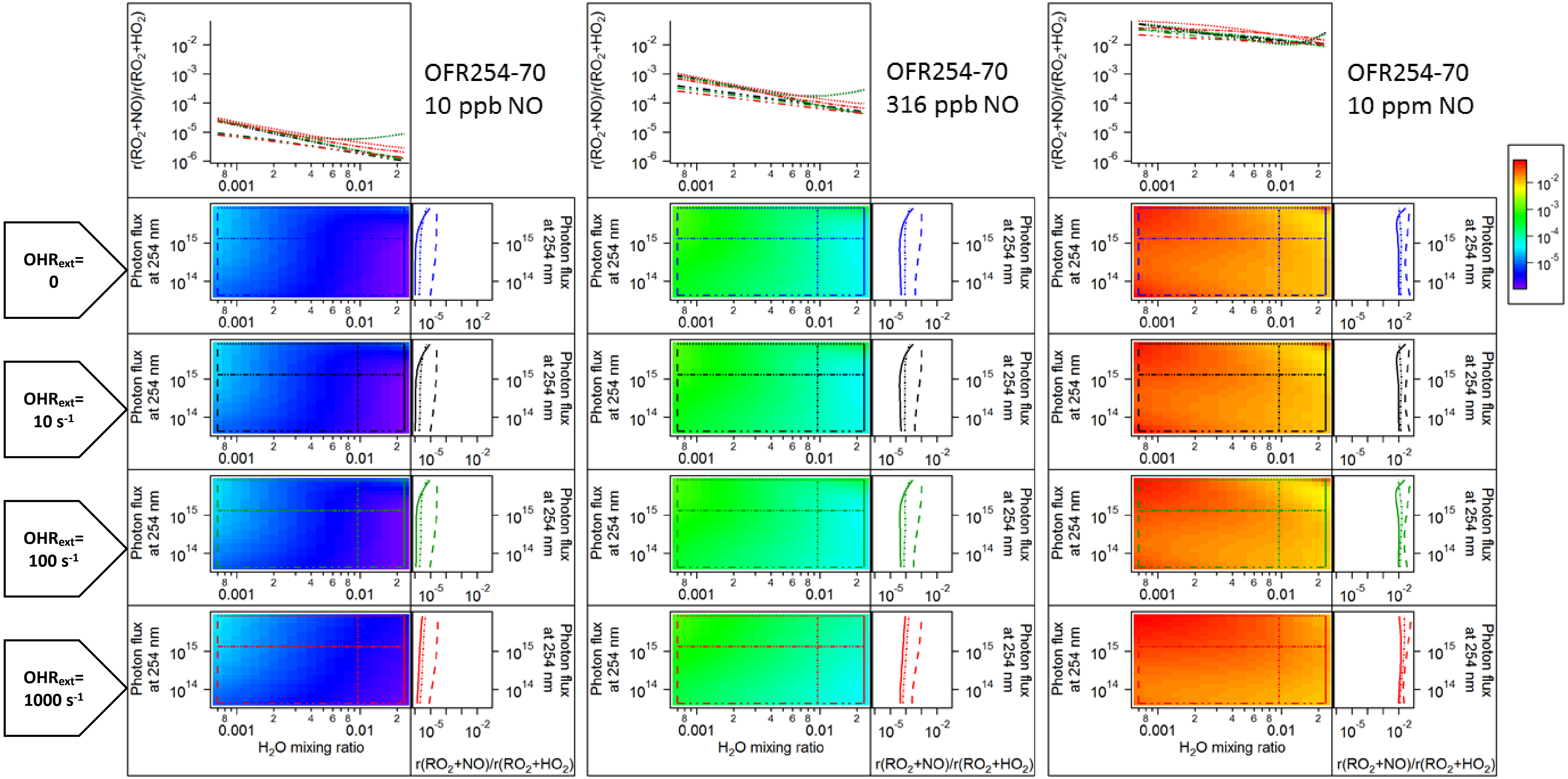

(f) r(RO_2+NO)/r(RO_2+HO_2) for OFR254-70-iNO

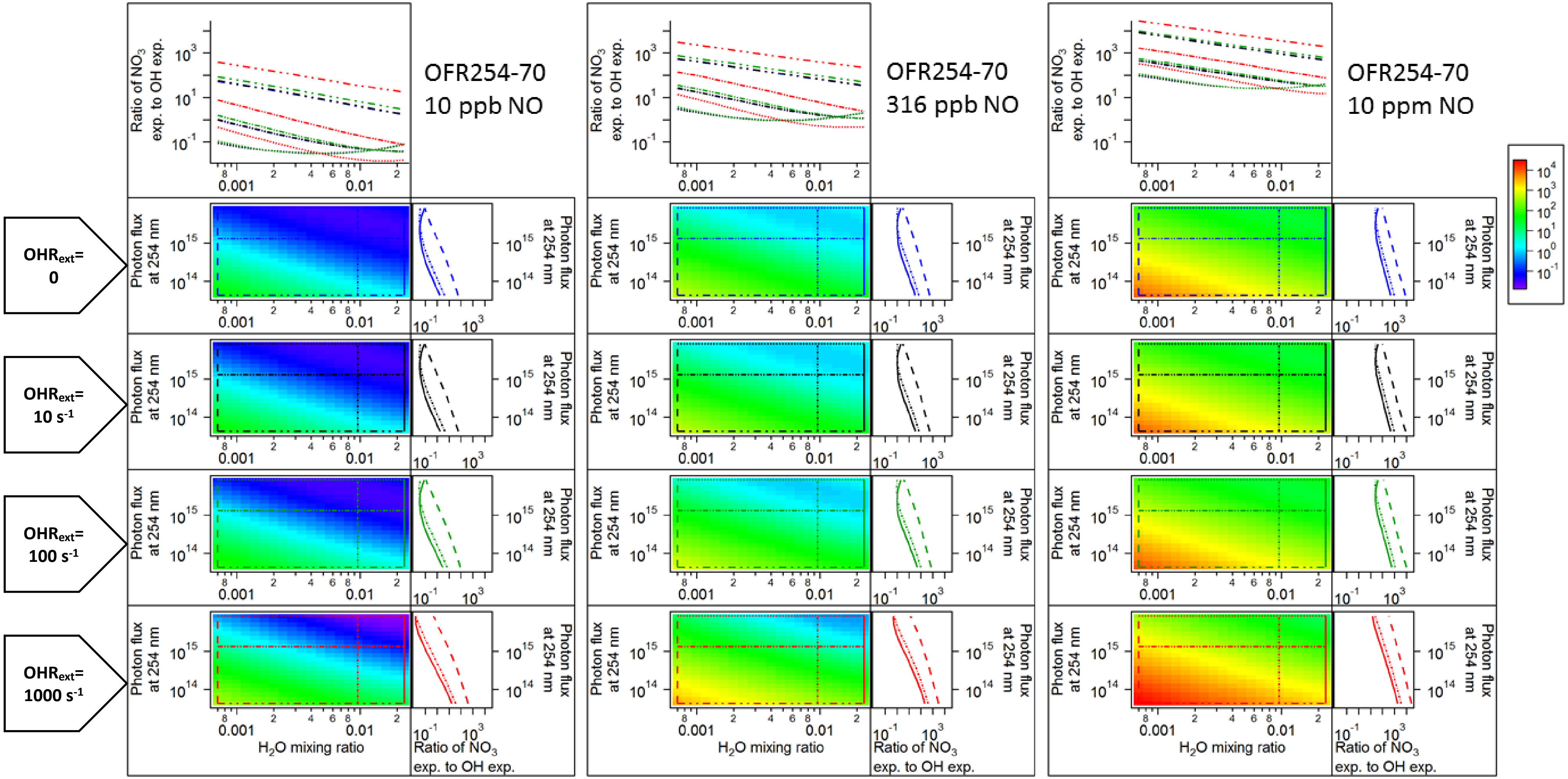

(g) NO_3 exposure/OH exposure for OFR254-70-iNO

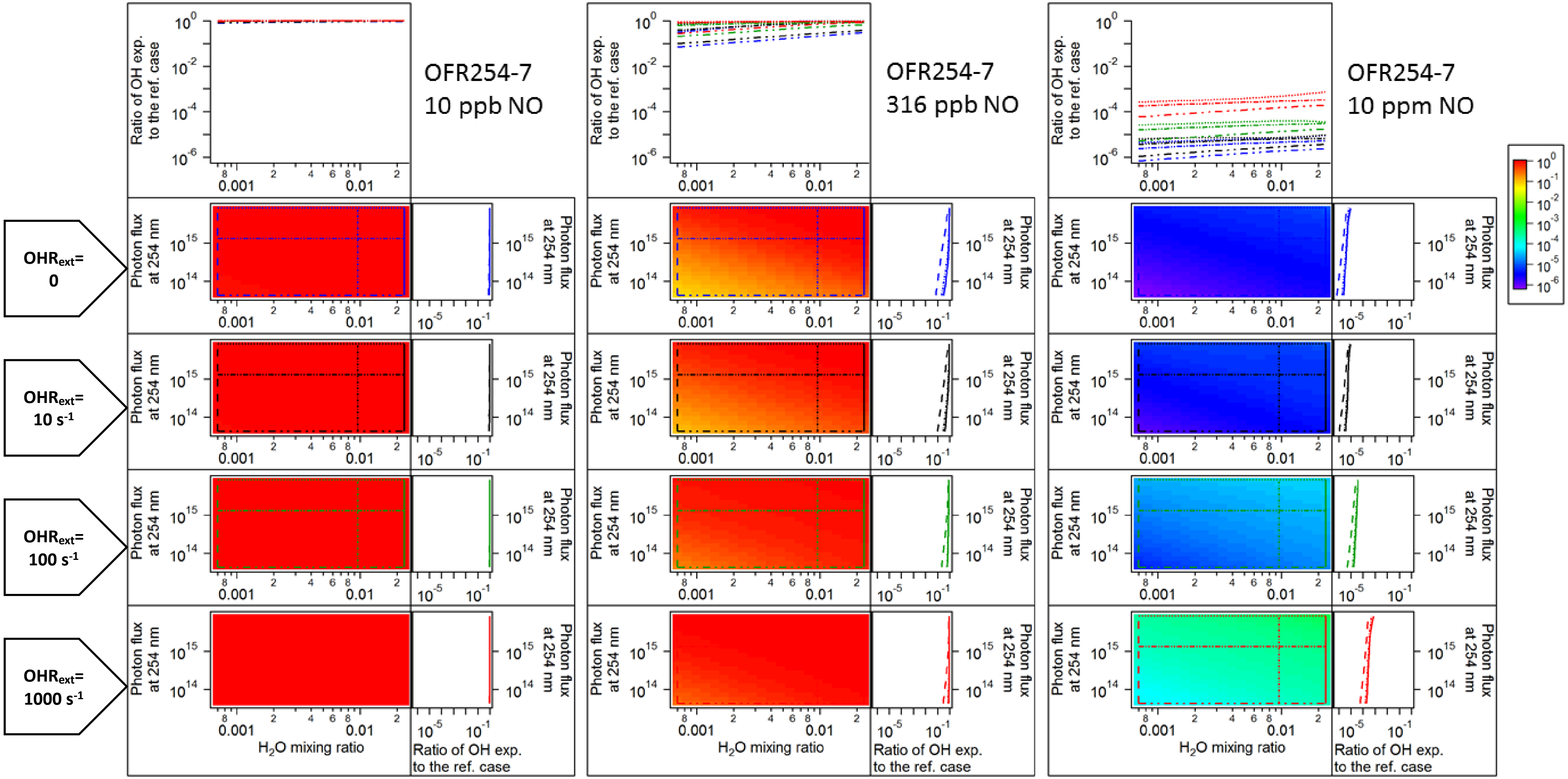

40

41 **(h) Ratio of OH exposure in the case with input NO to that in the corresponding case (same H_2O, UV, and OHR_{ext}) without input NO for OFR254-7-iNO**

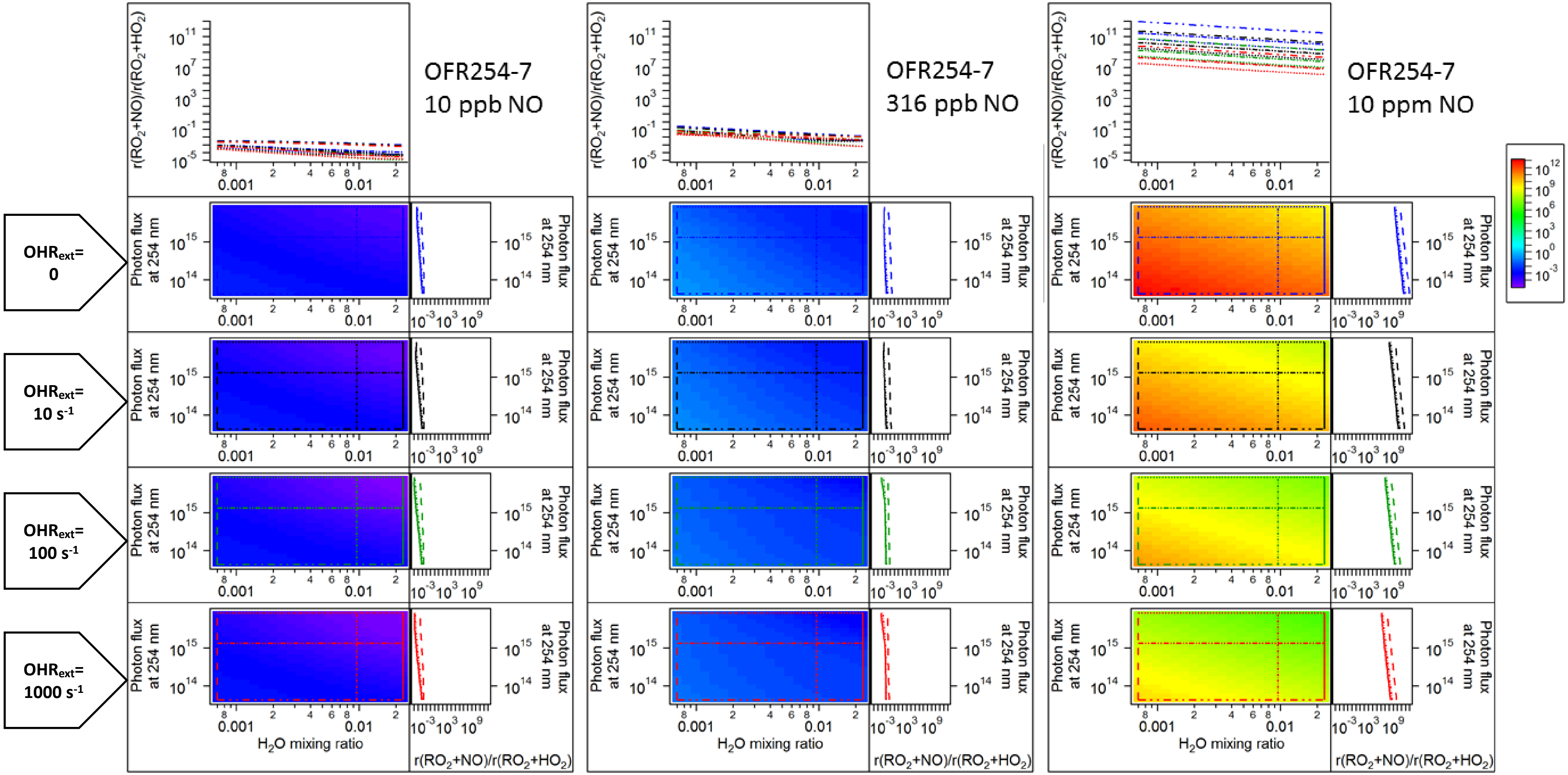

42
43 (i) $r(RO_2+NO)/r(RO_2+HO_2)$ for OFR254-7-iNO

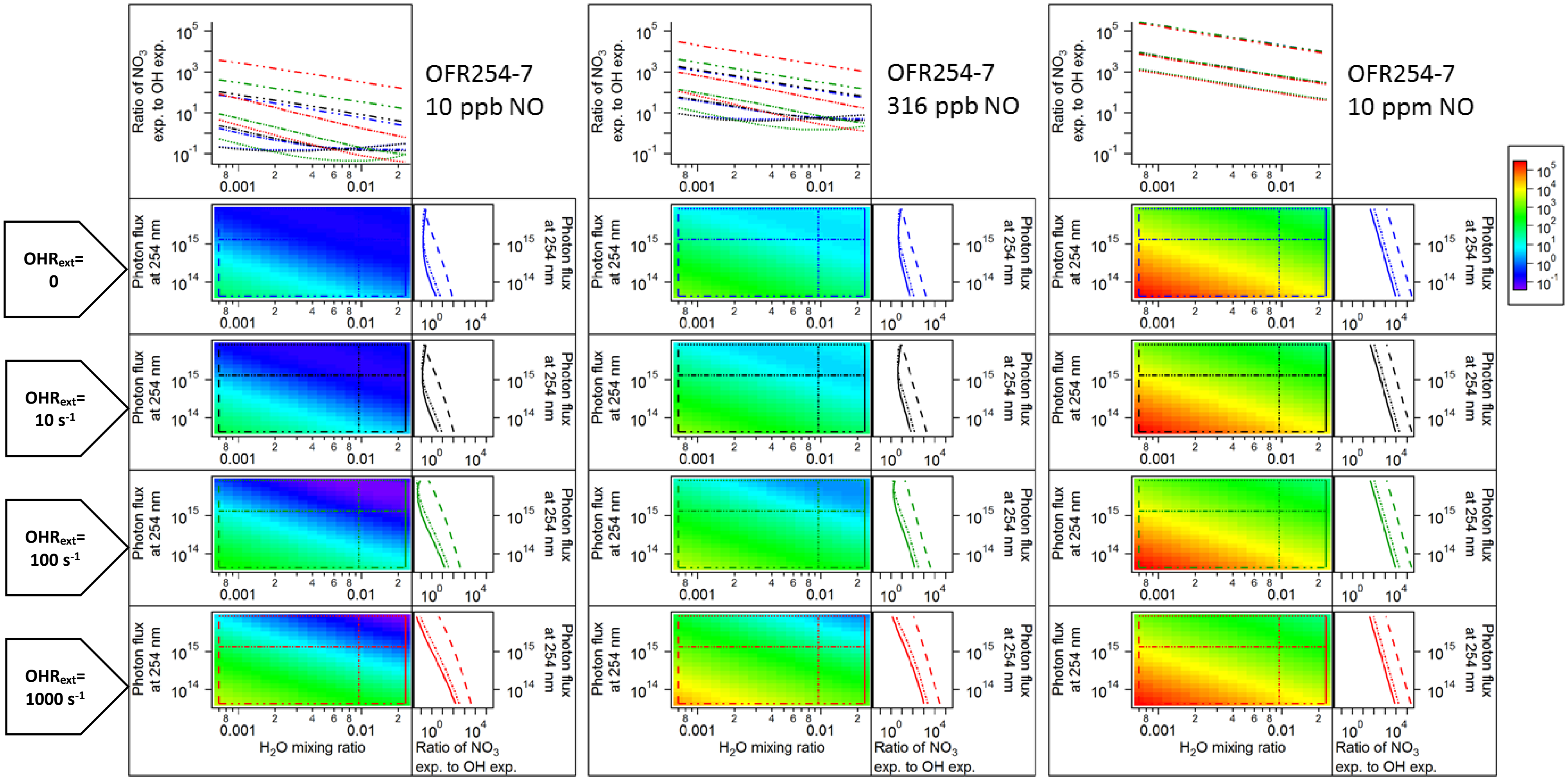

44
45 **(j) NO_3 exposure/OH exposure for OFR254-7-iNO**

Figure S3. Dependence of several quantities in OFR185-iNO, OFR254-70-iNO, and OFR254-7-iNO on H_2O and UV, for OHR_{ext} of 0, 10, 100, and 1000 s^{-1} (first, second, third, and fourth row of image plots in each multi-panel composite, respectively). Each multi-panel composite shows a quantity for OFR185-iNO, OFR254-70-iNO, or OFR254-7-iNO. The panels above and on the right of image plots are the line plots of the quantities shown in multi-panel composites in several typical cases. These cases are denoted in the image plots by horizontal or vertical lines of the same color and pattern as in the line plots.

In detail, the cut lines are in blue, black, dark green, and red in the plots for the cases of 0, low, high, and very high (0, 10, 100, and 1000 s^{-1}, respectively) external OH reactivity, respectively. Horizontal sparse-dash-dot-dot, dash-dot-dot, and dotted lines mark low, medium, and high water mixing ratios, respectively. Vertical dashed, dash-dot, and solid lines mark low, medium, and high photon fluxes, respectively. Refer to Table 2 for more details on case labels. Each multi-panel composite has a color scale corresponding to its image plots.

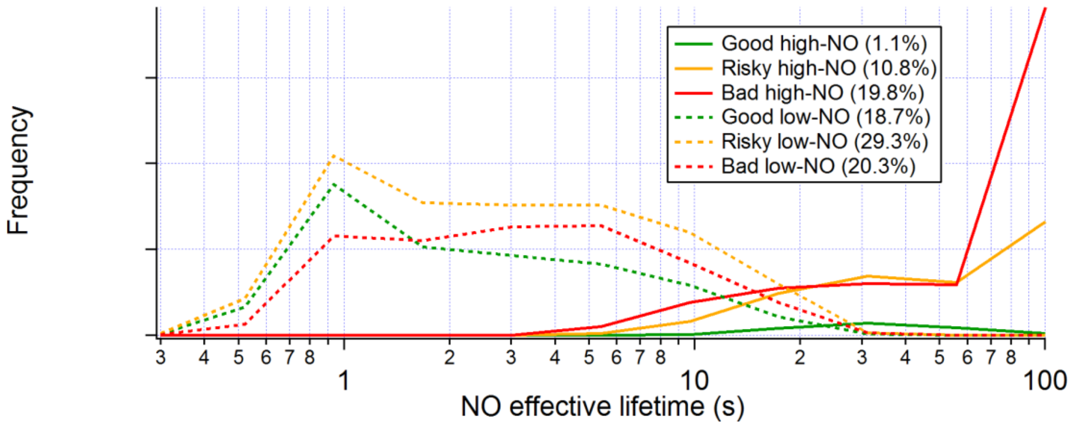

Figure S4. Frequency occurrence distributions of good/risky/bad high/low-NO conditions over NO effective lifetime for OFR185-iNO.

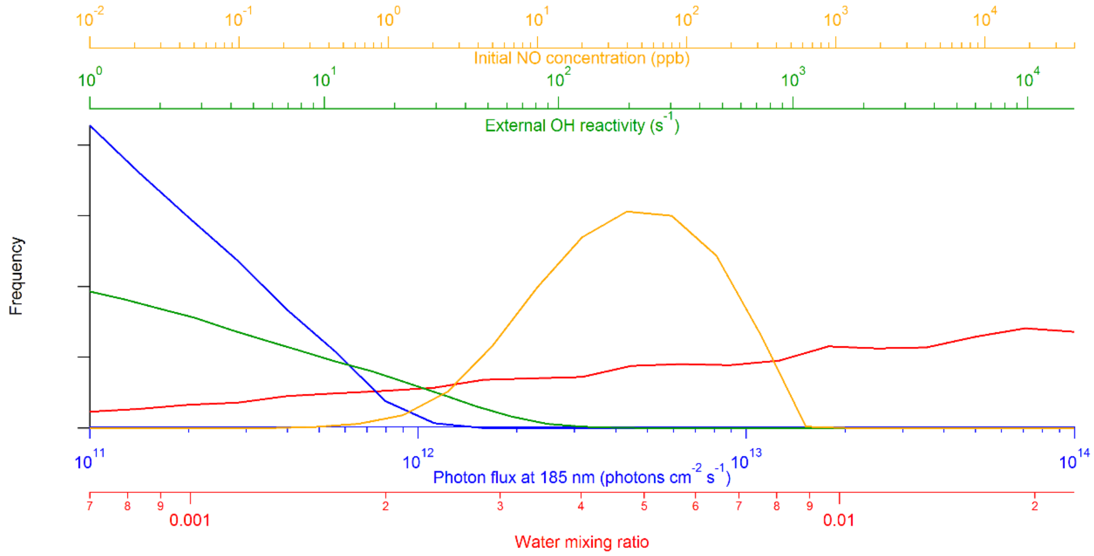

Figure S5. Frequency occurrence distributions of good high-NO conditions over physical inputs for OFR185-iNO.

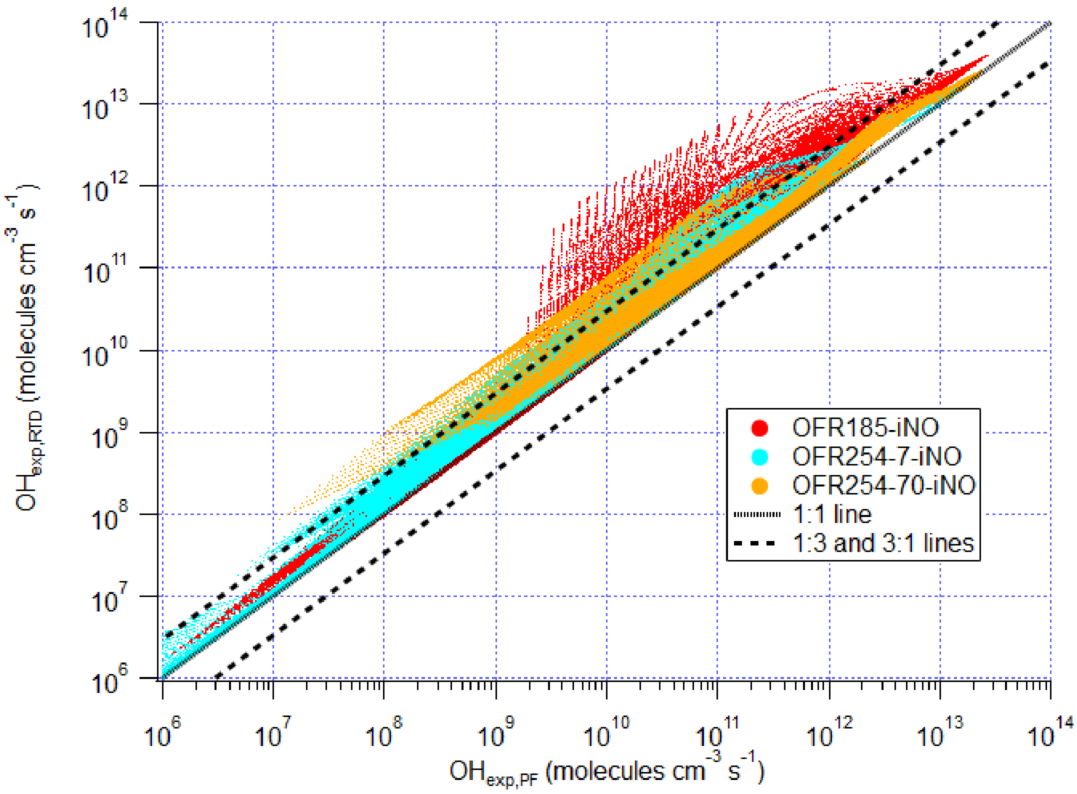

Figure S6. Scatter plot of OH exposure calculated in the model with the Lambe et al. (2011) residence time distribution ($OH_{exp,RTD}$) vs. that calculated in the plug-flow model ($OH_{exp,PF}$) for OFR185-iNO, OFR254-7-iNO, and OFR254-70-iNO. 1:1, 1:3, and 3:1 lines are also shown for comparison.

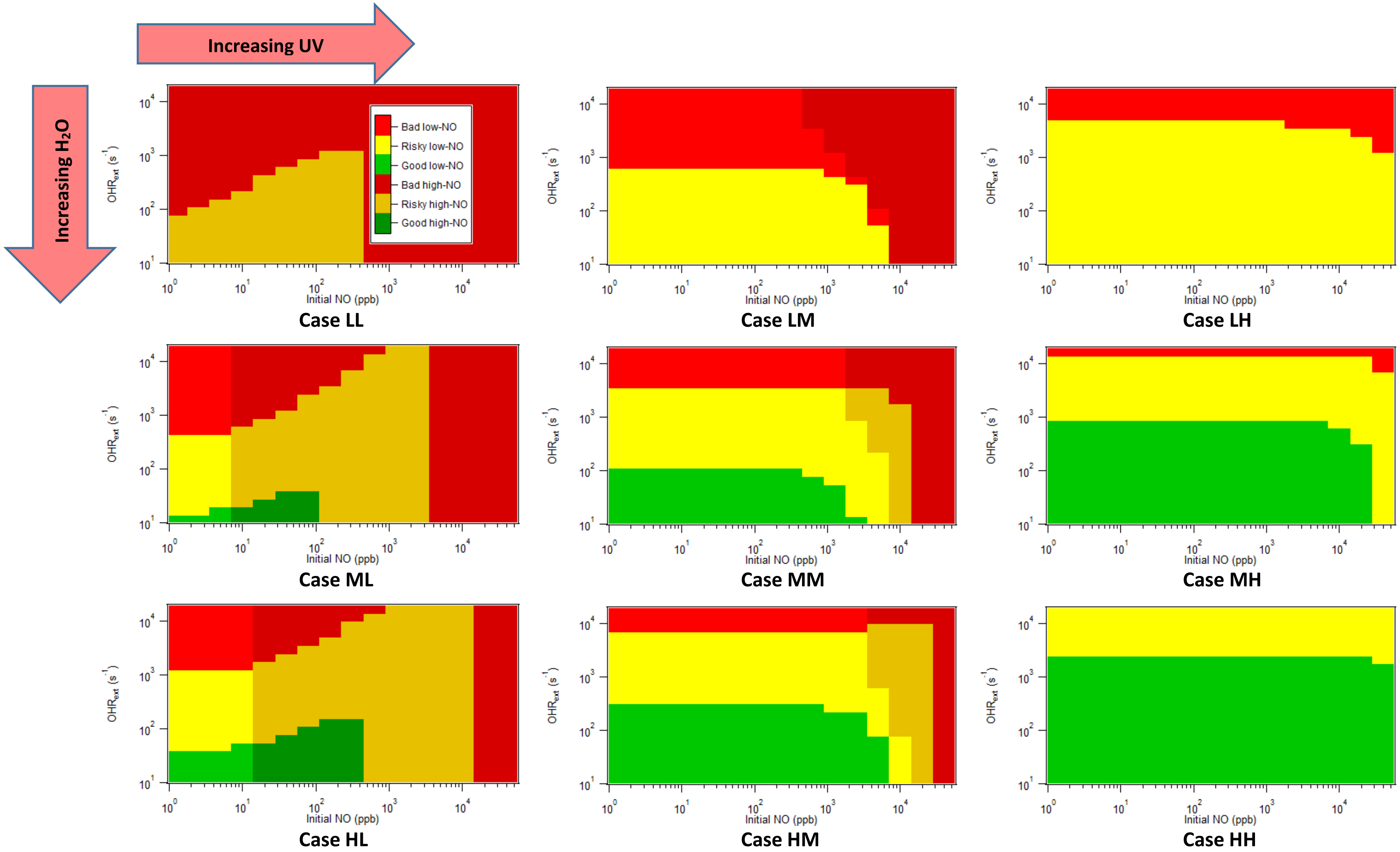

Increasing UV
Increasing H2O
Bad low-NO
Risky low-NO
Good low-NO
Bad high-NO
Risky high-NO
Good high-NO
OHRext (s-1)
Initial NO (ppb)
Case LL
Case LM
Case LH
Case ML
Case MM
Case MH
Case HL
Case HM
Case HH

Figure S7. Same format as Fig. 4, but for the OFR185-iNO results obtained by the model with the Lambe et al. (2011) residence time distribution.

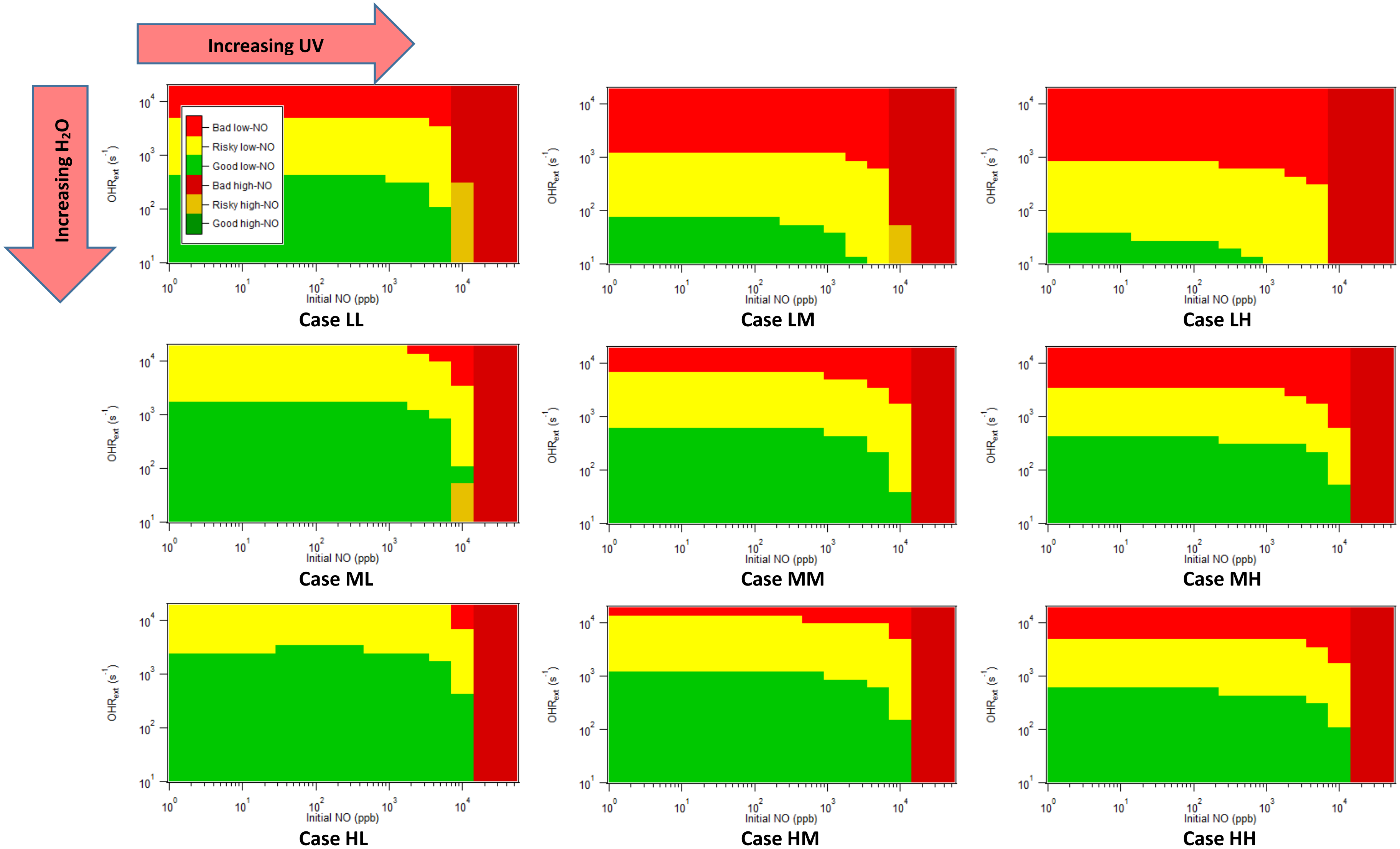

Increasing UV
Increasing H2O
Bad low-NO
Risky low-NO
Good low-NO
Bad high-NO
Risky high-NO
Good high-NO
OHRext (s-1)
Initial NO (ppb)
Case LL
Case LM
Case LH
Case ML
Case MM
Case MH
Case HL
Case HM
Case HH

Figure S8. Same format as Fig. 5, but for the OFR254-22-iNO results obtained by the model with the Lambe et al. (2011) residence time distribution.

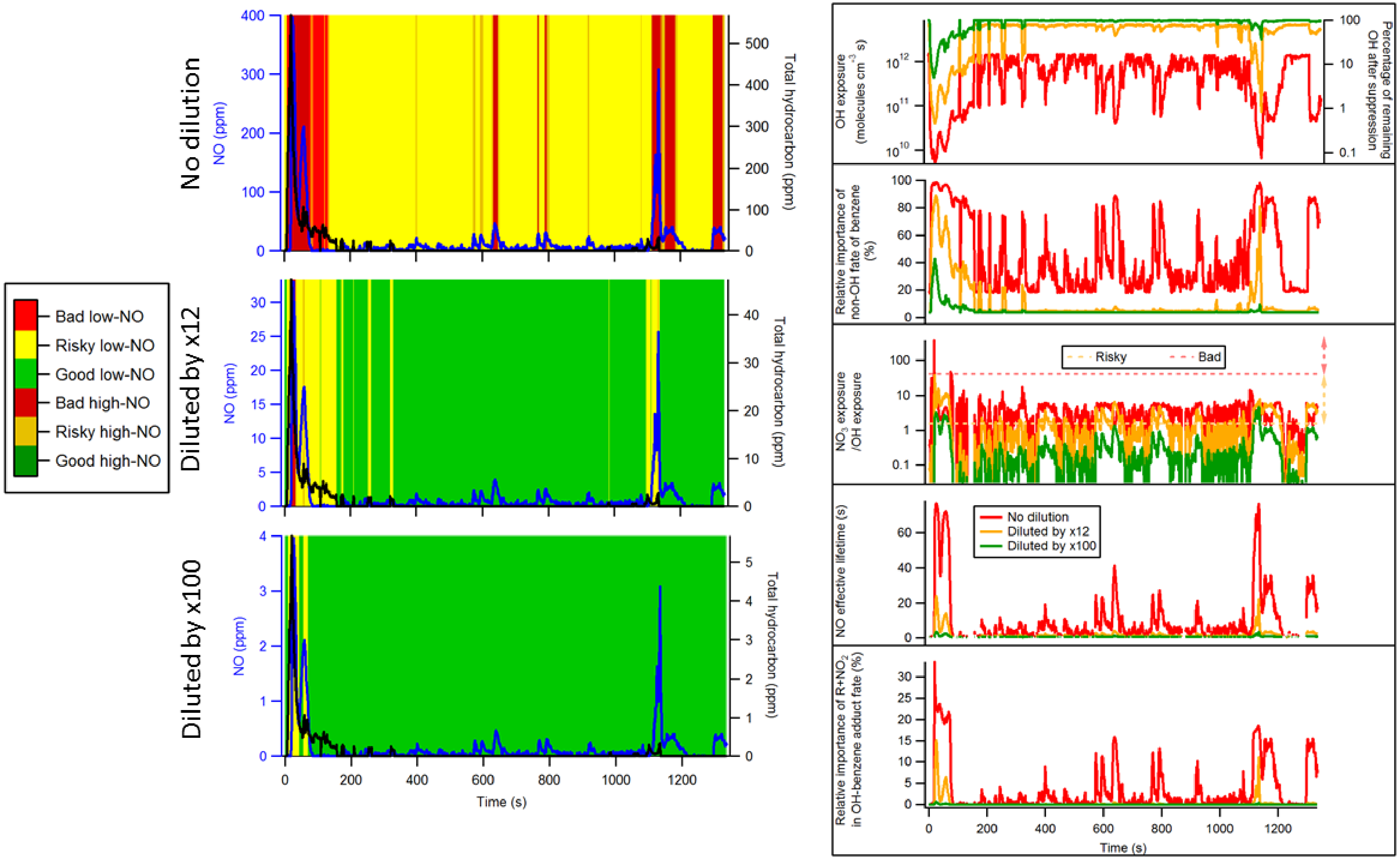

No dilution
Diluted by x12
Diluted by x100
NO (ppm)
Total hydrocarbon (ppm)
Time (s)
Bad low-NO
Risky low-NO
Good low-NO
Bad high-NO
Risky high-NO
Good high-NO
OH exposure (molecules cm^{-3} s)
Percentage of remaining OH after suppression
Relative importance of non-OH fate of benzene (%)
NO_3 exposure /OH exposure
Risky
Bad
NO effective lifetime (s)
No dilution
Diluted by x12
Diluted by x100
Relative importance of R+NO_2 in OH-benzene adduct fate (%)

Figure S9. Same as Fig. 7, but for the entire experiment (~1300 s).

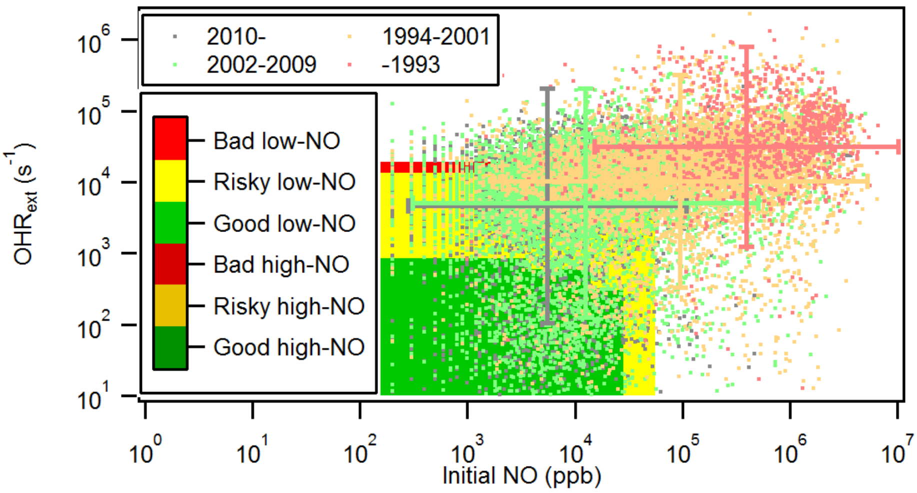

(a) Gasoline vehicles, no dilution (background: Case HH)

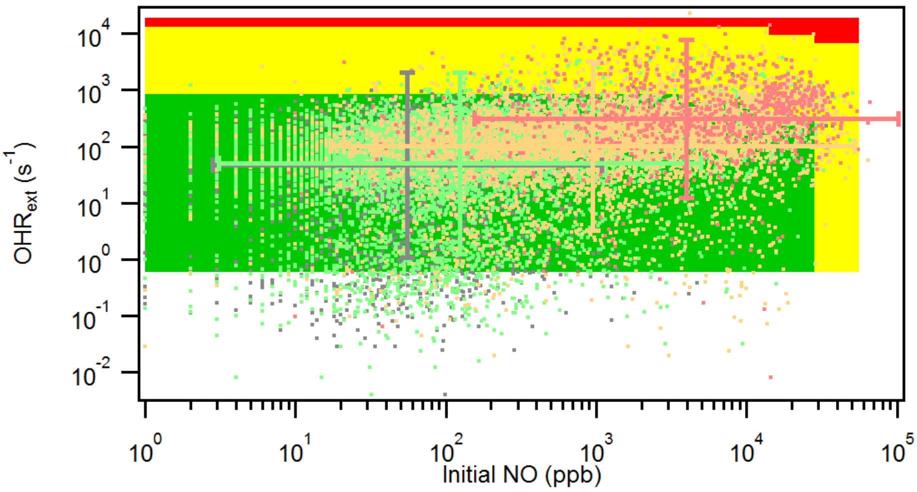

(b) Gasoline vehicles, dilution by a factor of 100 (background: Case HH)

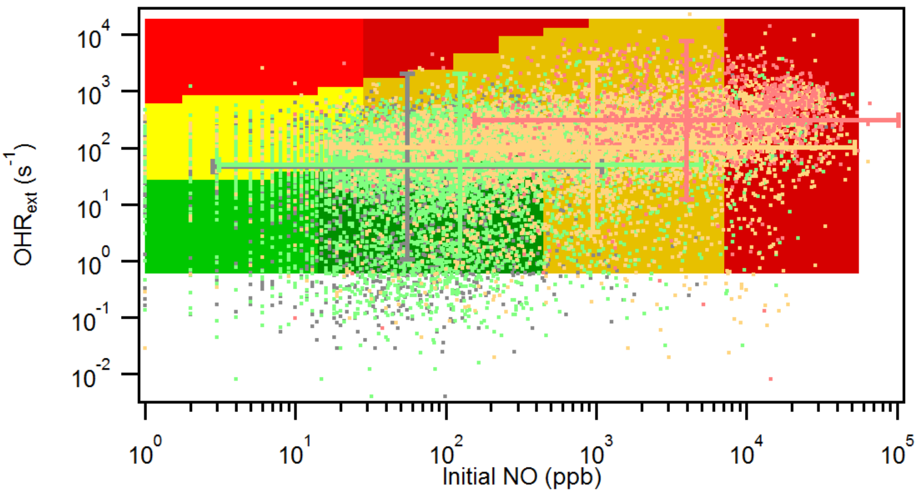

(c) Gasoline vehicles, dilution by a factor of 100 (background: Case HL)

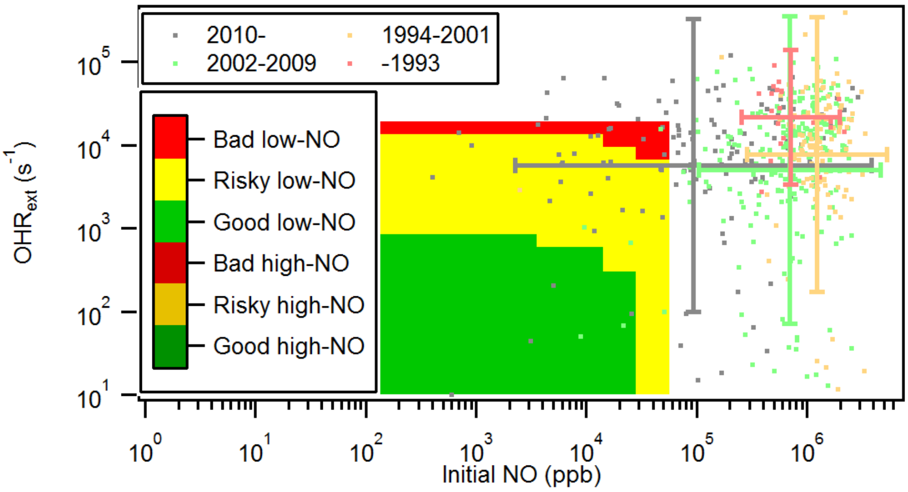

(d) Diesel vehicles, no dilution (background: Case HH)

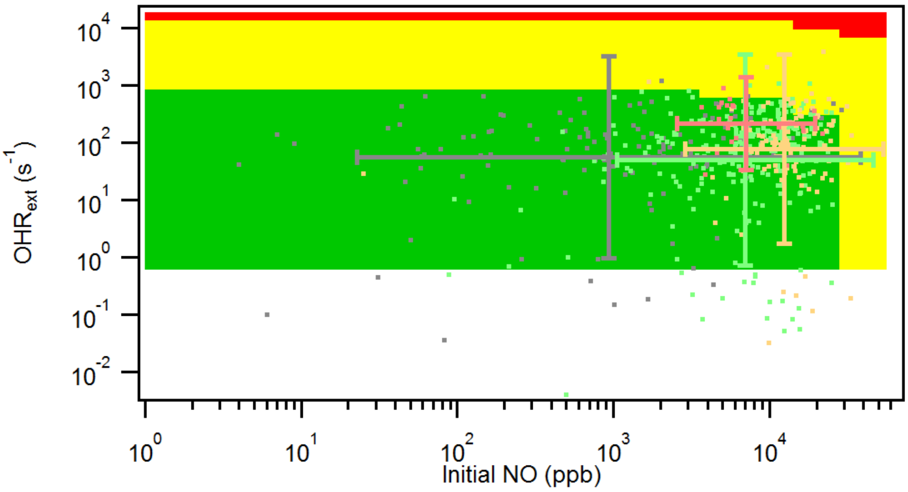

(e) Diesel vehicles, dilution by a factor of 100 (background: Case HH)

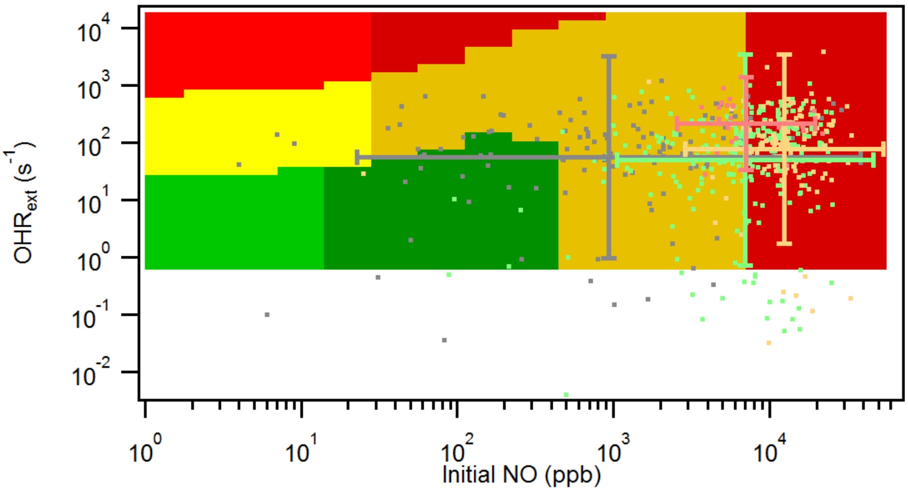

(f) Diesel vehicles, dilution by a factor of 100 (background: Case HL)

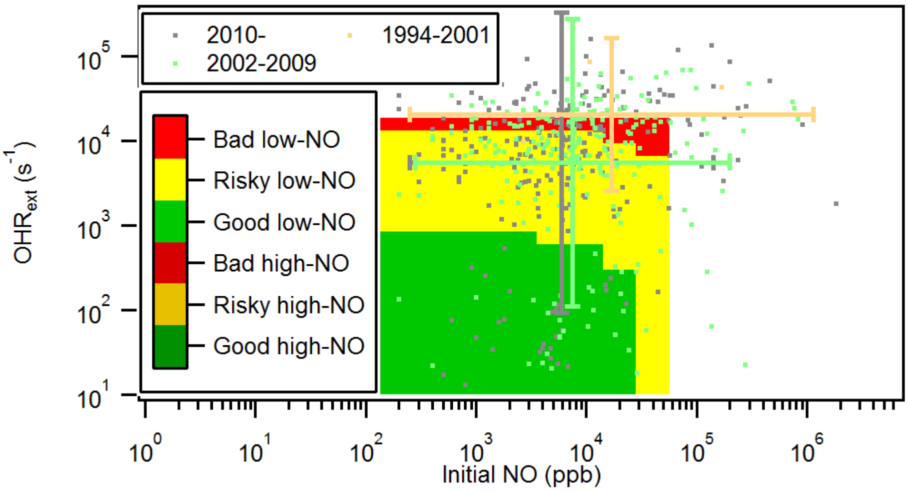

(g) Hybrid vehicles, no dilution (background: Case HH)

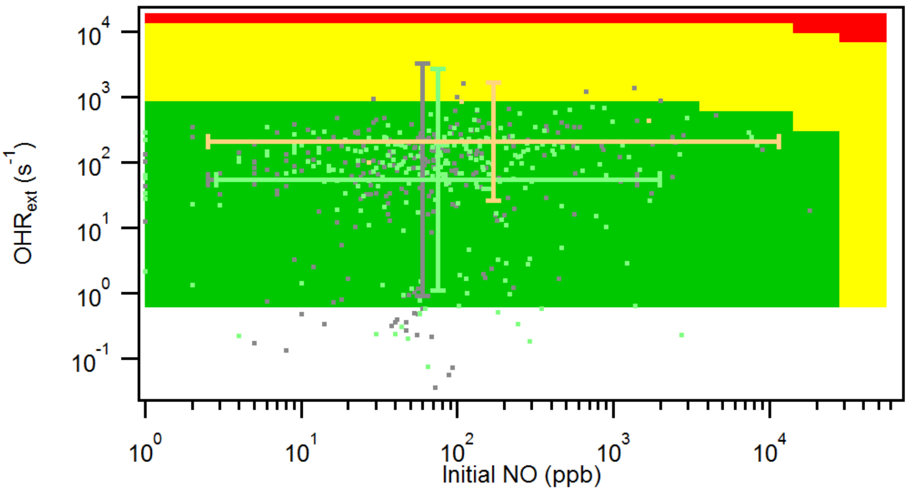

(h) Hybrid vehicles, dilution by a factor of 100 (background: Case HH)

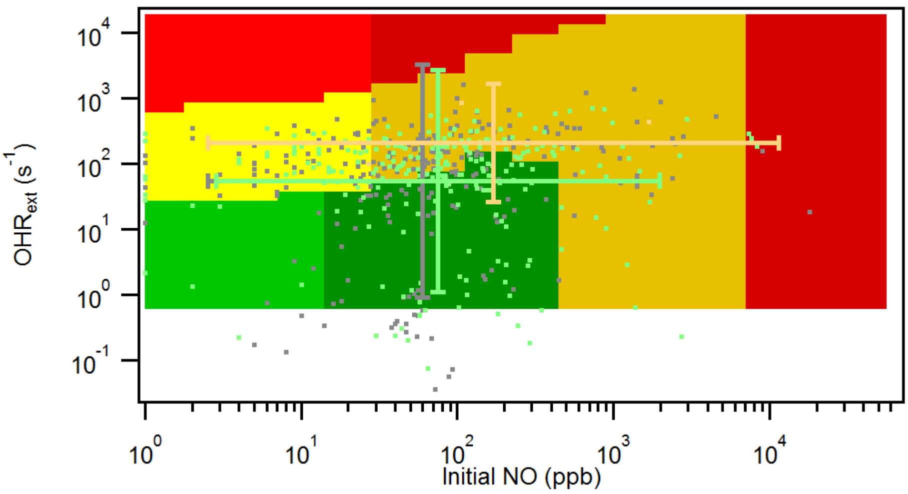

(i) Hybrid vehicles, dilution by a factor of 100 (background: Case HL)

Figure S10. Similar format as Fig. 9, but without the points for the test of Karjalainen et al. (2016) and with the scatter points of emissions of individual vehicles measured by Bishop and Stedman (2013). In addition to (a–c) the scatter points of emissions of gasoline vehicles, those of (d–f) diesel and (g–i) hybrid vehicles measured by Bishop and Stedman (2013) are also shown.

S1. Rationale for selecting the criterion to quantify "high-NO" vs. "low-NO" conditions

A "high-NO" condition results in more RO_2 reacted with NO than with HO_2. The amount of RO_2 reacted with NO, r(RO_2+NO), is the integral of the rate of this reaction over the entire residence time, i.e.,

$$\mathrm{r}(\mathrm{RO_2{+}NO}) = \int_0^{t_{res}} k(\mathrm{RO_2{+}NO})[\mathrm{RO_2}]\,[\mathrm{NO}]dt,$$

where t_{res} is residence time, k(RO_2+NO) is the rate constant of the reaction RO_2+NO, and [RO_2] and [NO] are RO_2 and NO concentrations, respectively. The entire residence time is taken into account since there is still significant presence of VOCs after NO and primary VOCs are destroyed. The oxidation intermediates/products of primary VOCs can exist for a much longer period than NO lifetime (Nehr et al., 2014; Schwantes et al., 2017). In addition, heterogeneous OA oxidation can be important at high photochemical ages in OFR (Hu et al., 2016), leading to decomposition and revolatilization of particle-phase species. Thus continuing oxidation processes are very likely to occur during the entire the residence time.

[RO_2] under a steady state approximation can be expressed as below

$$[\mathrm{RO_2}] = \frac{\mathrm{OHR_{VOC}}[\mathrm{OH}]}{k(\mathrm{RO_2{+}NO})[\mathrm{NO}] + k(\mathrm{RO_2{+}HO_2})[\mathrm{HO_2}] + k(\mathrm{RO_2{+}RO_2'})[\mathrm{RO_2'}] + \cdots},$$

where the numerator and denominator on the right side are respectively the RO_2 production rate and its total first-order RO_2 loss rate constant. The production rate is simply the product of OH concentration [OH] and OHR of VOC OHR_{VOC}. The total loss rate constant is the sum of those of all RO_2 fates (RO_2+NO, RO_2+HO_2, RO_2+RO_2',…).

We neglect all minor RO_2 fates. RO_2+RO_2' is also neglected since RO_2+RO_2' cannot compete with RO_2+NO and RO_2+HO_2 for most RO_2 (Orlando and Tyndall, 2012), including under the typical OFR conditions, and also to focus on the relative importance of RO_2+NO and RO_2+HO_2. As k(RO_2+NO) and k(RO_2+HO_2) are very similar (Orlando and Tyndall, 2012), we assume k(RO_2+NO)=k(RO_2+HO_2)=k. Then the [RO_2] estimation expression can be simplified as

$$[\mathrm{RO_2}] \approx \frac{\mathrm{OHR_{VOC}}[\mathrm{OH}]}{k[\mathrm{NO}] + k[\mathrm{HO_2}]}.$$

Because OHR from VOC (including the reactivity of the products of the initial VOC(s)) is relatively stable for most OFR experiments (Peng et al., 2015), OHR_{VOC} is assumed to be constant here. Then r(RO_2+NO) can be rearranged as below

$$\mathrm{r}(\mathrm{RO_2{+}NO}) = \mathrm{OHR_{VOC}} \int_0^{t_{res}} \frac{[\mathrm{OH}][\mathrm{NO}]}{[\mathrm{NO}] + [\mathrm{HO_2}]} dt.$$

Similarly, the amount of RO_2 reacted with HO_2, r(RO_2+HO_2), can be obtained

$$\mathrm{r}(\mathrm{RO_2{+}HO_2}) = \mathrm{OHR_{VOC}} \int_0^{t_{res}} \frac{[\mathrm{OH}][\mathrm{HO_2}]}{[\mathrm{NO}] + [\mathrm{HO_2}]} dt.$$

Finally, we define "high-NO" conditions as those satisfying:

$$\mathrm{r(RO_2{+}NO)} > \mathrm{r(RO_2{+}HO_2)}$$

i.e.,

$$\frac{\mathrm{r(RO_2{+}NO)}}{\mathrm{r(RO_2{+}HO_2)}} = \int_0^{t_{res}} \frac{[\mathrm{OH}][\mathrm{NO}]}{[\mathrm{NO}] + [\mathrm{HO_2}]} dt \Big/ \int_0^{t_{res}} \frac{[\mathrm{OH}][\mathrm{HO_2}]}{[\mathrm{NO}] + [\mathrm{HO_2}]} dt > 1$$

The ratio between the two integrals on the left side of the inequality can be calculated by the model used in the present study. We thus take this inequality as the criterion for high-NO conditions in this study.

References

Bishop, G. A. and Stedman, D. H.: Fuel Efficiency Automobile Test: Light-Duty Vehicles, [online] Available from: http://www.feat.biochem.du.edu/light_duty_vehicles.html (Accessed 1 February 2017), 2013.

Hu, W., Palm, B. B., Day, D. A., Campuzano-Jost, P., Krechmer, J. E., Peng, Z., de Sá, S. S., Martin, S. T., Alexander, M. L., Baumann, K., Hacker, L., Kiendler-Scharr, A., Koss, A. R., de Gouw, J. A., Goldstein, A. H., Seco, R., Sjostedt, S. J., Park, J.-H., Guenther, A. B., Kim, S., Canonaco, F., Prévôt, A. S. H., Brune, W. H. and Jimenez, J. L.: Volatility and lifetime against OH heterogeneous reaction of ambient isoprene-epoxydiols-derived secondary organic aerosol (IEPOX-SOA), Atmos. Chem. Phys., 16(18), 11563–11580, doi:10.5194/acp-16-11563-2016, 2016.

Karjalainen, P., Timonen, H., Saukko, E., Kuuluvainen, H., Saarikoski, S., Aakko-Saksa, P., Murtonen, T., Bloss, M., Dal Maso, M., Simonen, P., Ahlberg, E., Svenningsson, B., Brune, W. H., Hillamo, R., Keskinen, J. and Rönkkö, T.: Time-resolved characterization of primary particle emissions and secondary particle formation from a modern gasoline passenger car, Atmos. Chem. Phys., 16(13), 8559–8570, doi:10.5194/acp-16-8559-2016, 2016.

Lambe, A. T., Ahern, A. T., Williams, L. R., Slowik, J. G., Wong, J. P. S., Abbatt, J. P. D., Brune, W. H., Ng, N. L., Wright, J. P., Croasdale, D. R., Worsnop, D. R., Davidovits, P. and Onasch, T. B.: Characterization of aerosol photooxidation flow reactors: heterogeneous oxidation, secondary organic aerosol formation and cloud condensation nuclei activity measurements, Atmos. Meas. Tech., 4(3), 445–461, doi:10.5194/amt-4-445-2011, 2011.

Nehr, S., Bohn, B., Fuchs, H., Häseler, R., Hofzumahaus, A., Li, X., Rohrer, F., Tillmann, R. and Wahner, A.: Atmospheric photochemistry of aromatic hydrocarbons: OH budgets during SAPHIR chamber experiments, Atmos. Chem. Phys., 14(13), 6941–6952, doi:10.5194/acp-14-6941-2014, 2014.

Orlando, J. J. and Tyndall, G. S.: Laboratory studies of organic peroxy radical chemistry: an overview with emphasis on recent issues of atmospheric significance, Chem. Soc. Rev., 41(19), 6294, doi:10.1039/c2cs35166h, 2012.

Peng, Z., Day, D. A., Stark, H., Li, R., Lee-Taylor, J., Palm, B. B., Brune, W. H. and Jimenez, J. L.: HOx radical chemistry in oxidation flow reactors with low-pressure mercury lamps systematically examined by modeling, Atmos. Meas. Tech., 8(11), 4863–4890, doi:10.5194/amt-8-4863-2015, 2015.

Schwantes, R. H., Schilling, K. A., McVay, R. C., Lignell, H., Coggon, M. M., Zhang, X., Wennberg, P. O. and Seinfeld, J. H.: Formation of highly oxygenated low-volatility products from cresol oxidation, Atmos. Chem. Phys., 17(5), 3453–3474, doi:10.5194/acp-17-3453-2017, 2017.